Ceramics International 47 (2021) 11209–11219

Contents lists available at ScienceDirect

Ceramics International

journal homepage: www.elsevier.com/locate/ceramint

Development and characterisation of microporous biomimetic scaffolds loaded with magnetic nanoparticles as bone repairing material

Florina D. Cojocaru [a,b,2,1], Vera Balan [b,1], Constantin-Edi Tanase [b,*,3,1], Ionel Marcel Popa [a], Maria Butnaru [b], Ovidiu Bredetean [b], Mihai Mares [e], Valentin Nastasa [e], Sorin Pasca [f], Liliana Verestiuc [b,**]

[a] Faculty of Chemical Engineering and Environmental Protection, Department of Chemical Engineering, Gheorghe Asachi Technical University, Iasi, Romania
[b] Faculty of Medical Bioengineering, Department of Biomedical Sciences, Grigore T. Popa University of Medicine and Pharmacy, Iasi, Romania
[e] Laboratory of Antimicrobial Chemotherapy, Ion Ionescu de La Brad University of Agricultural Sciences and Veterinary Medicine, Iasi, Romania
[f] Laboratory of Pathological Anatomy, Ion Ionescu de La Brad University of Agricultural Sciences and Veterinary Medicine, Iasi, Romania

ARTICLE INFO

Keywords:
Biopolymers
SPIONs
Calcium phosphates
Composite biomaterials
Bone scaffolds

ABSTRACT

Fine-tuning of the scaffolds structural features for bone tissue engineering can be an efficient approach to regulate the specific response of the osteoblasts. Here, we loaded magnetic nanoparticles aka superparamagnetic iron oxide nanoparticles (SPIONs) into 3D composite scaffolds based on biological macromolecules (chitosan, collagen, hyaluronic acid) and calcium phosphates for potential applications in bone regeneration, using a biomimetic approach. We assessed the effects of organic (chitosan/collagen/hyaluronic acid) and inorganic (calcium phosphates, SPIONs) phase over the final features of the magnetic scaffolds (MS). Mechanical properties, magnetic susceptibility and biological fluids retention are strongly dependent on the final composition of MS and within the recommended range for application in bone regeneration. The MS architecture/pore size can be made bespoken through changes of the final organic/inorganic ratio. The scaffolds undertake mild degradation as the presence of inorganic components hinders the enzyme catalytic activity. *In vitro* studies indicated that osteoblasts (SaOS-2) on MS9 had similar cell behaviour activity in comparison with the TCP control. *In vivo* data showed an evident development of integration and resorption of the MS composites with low inflammation activity. Current findings suggest that the combination of SPIONs into 3D composite scaffolds can be a promising toolkit for bone regeneration.

1. Introduction

Bone is the second most transplanted tissue worldwide, with at least two million procedures annually using bone grafts and bone substitute materials [1,2]. Diseases such as osteoarthritis, osteoporosis or Paget's disease and traumatic injuries can damage normal bone functions and lead to harsh pain, immobility, bone fractures and deformity. Despite the natural capacity of bone healing, current clinical treatments used for large bone defects are still challenging. For example, if an injury is beyond a critical limit (critical size defect), it cannot heal by itself and, in this case, patients need invasive surgical intervention to aid bone regeneration. This can involve clinical use of bone grafts, bone substitute materials, growth factors, free fibula vascularized grafts and insertion of metal plates, wires and pins to support stability and bone regeneration [3–7]. Bone tissue engineering offers promising alternatives for reconstructing critical tissue defects resulted from trauma, tumour, resection and skeletal abnormalities. These approaches involve the use of biomimetic and biodegradable scaffolds as a pattern for cell growth and

* Corresponding author.
** Corresponding author.
E-mail addresses: cetanase@cantab.net (C.-E. Tanase), iliana.verestiuc@bioinginerie.ro (L. Verestiuc).
[1] Authors with equal contribution.
[2] current affiliation: Advanced Centre for Research-Development in Experimental Medicine, Grigore T. Popa University of Medicine and Pharmacy of Iasi, Romania.
[3] current affiliation: Immunology & Immuno-Bioengineering Group, School of Life Sciences, University of Nottingham, University Park, Nottingham, NG7 2RD, United Kingdom.

https://doi.org/10.1016/j.ceramint.2020.12.246
Received 24 September 2020; Received in revised form 21 December 2020; Accepted 24 December 2020
Available online 30 December 2020

extracellular matrix deposition in order to restore both functional and mechanical properties of the native tissue [8–11].

Various materials have been investigated with the aim to substitute the natural bone. Among them, synthetic and inorganic ceramic materials (e.g. hydroxyapatite-Hap and tricalcium phosphate-TCP, bicalcium phosphates-BCP) endowed with osteoconductive properties can mimic the physical attributes of the bone [12–15], but the porous ceramics are innately brittle and exhibits low mechanical properties of bone restraining their clinical relevance as synthetic bone scaffolds. Therefore, natural polymers such as: collagen (Col), chitosan (Cs) and hyaluronic acid (Hya) and their combinations with calcium phosphates (CP) are considered an attractive and versatile alternative for development of biomimetic and biodegradable bone scaffolds [16–21]. In the same time, creating a 3D scaffold with controlled internal architecture imply the use of specific procedures such as gel casting, 3D printing, drying and freeze-drying, crosslinking, etc [22–27]. Among them, freeze-drying enables the formation of 3D porous structures with various morphological structures allowing cell attachment, proliferation, infiltration, nutrient diffusion, etc. making this a valuable approach in development of ice template scaffolds for tissue engineering [28–30]. To address specific requirements, a 3D bone scaffold must: i) provide temporary mechanical support to the affected area; ii) act as a substrate for osteoid deposition; iii) have a porous architecture to allow encourage bone cell migration, bone in-growth and vascularisation; iv) support and promote osteogenic differentiation in the non-osseous, synthetic scaffold (osteoinduction); v) enhance cellular activity towards scaffold-host tissue integration (osseointegration); vi) degrade in a controlled manner to facilitate the bone growth; vii) generate non-toxic degradation products; viii) not induce any innate or chronic inflammatory response; ix) be suitable for sterilization without the loss of bioactivity; x) deliver bioactive molecules or drugs in a controlled manner to accelerate healing and prevent further pathologies [31,32].

More than that, bone engineered scaffolds need to be driven by a personal medicine approach and must integrate a range of biological and physical properties for optimal bone regeneration [33]. Recent studies have shown that addition of SPIONs to composite scaffolds based on polymers and ceramics, supports osteoblasts proliferation and rapid bone regeneration, with or without magnetic stimulation [34–42]. SPIONS are able to increase the cell growth by suppressing the intracellular H_2O_2 [43], to induce osteogenesis by activating the classic mitogen-activated protein kinase (MAPK) signal pathway and to promote the osteogenic differentiation [44]. Furthermore, SPIONs are used due to their properties such as hyperthermia and/or chemotherapeutics capabilities [45,46], features that can be useful for the treatment of bone tissue defects induced by bone tumours.

In this paper, we developed composites microporous biomimetic scaffolds loaded with SPIONs, denoted as MS and explored the influence of three biopolymers (Cs, Col, Hya) composition over the final characteristics of the MS (e.g. simulated biological fluids retention, enzymatic degradation, pore size, mechanical and magnetic properties). Biomimetic procedure that controls the pH and temperature of the CP precipitation, from its precursors, directly in the biopolymer-SPIONs mixture can tailor the final MS properties. We further explored *in vitro* and *in vivo* behaviour of MS as prospective substrates for bone regeneration.

2. Materials and methods

2.1. Materials

Two polysaccharides (chitosan - Cs, CAS: 9,012,764 and hyaluronic acid, sodium salt -Hya, CAS: 9,067,327), one protein (type I collagen - Col, kindly donated by Lohmann &Rauscher GmbH, Germany), calcium phosphates - CP precursors (calcium chloride – $CaCl_2{\cdot}2H_2O$, CAS: 10,035,048 and monosodium phosphate - $NaH_2PO_4{\cdot}2H_2O$, CAS: 13,472,350) and magnetite coated with Cs, denoted as SPIONs colloidal suspension have been used for scaffolds preparation. Retention of simulated body fluids studies have been performed with phosphate buffered solutions - PBS, pH = 7.4, 0.01 M, used also for *in vitro* degradation studies together with lysozyme (CAS: 12,650,883), potassium ferricyanide - $K_3Fe(CN)_6$ (CAS: 13,746,662), collagenase clostridium histolyticum (CAS: 9,001,121) and ninhydrin reagent (CAS: 485,472).

2.2. Scaffolds preparation

The MS have been obtained by mixing the biopolymers solutions (Cs, Col, Hya) with a SPIONs colloidal suspension (prepared in our group) [47]. According to previously results regarding composites based on biopolymers with SPIONs included (in various concentrations, namely 1%, 3% and respectively 5%), with suitable magnetic properties for bone tissue engineering applications [48], we have selected a concentration of 5 wt % SPIONs suspension (SPIONS with an average mean diameter of 154 ± 4 nm). The default concentration of the biopolymers was 1% for Cs, Col and Hya (the last one was 5%, wt/wt reported to Cs-Col). Within the final composition of the MS the Cs-Col ratio and Ca/P ratio was changed based on the details of the experimental program (Table 1).

Briefly, the biopolymers solutions and SPIONs were mixed with different amounts of CP precursors (CaCl2-40% and NaH2PO4-25%) and co-precipitated with ammonia aqueous solution (NH4OH-25%) maintaining a 7.2 pH for 24 h. The final mixture was intensively washed with distilled water and centrifuged at 5000 rpm for 10 min three times and subsequently poured into silicon moulds (diameter 3 cm) and freeze-dried. Freeze-drying was carried out with a FreeZone benchtop freeze-drier (Labconco, US), using a constant cooling rate of 1 °C min^{-1} to a final freezing temperature of −55 °C. The temperature was held for 24 h to ensure freezing was complete, at which point the ice was sublimed under a vacuum of 41mTorr at 0 °C. UV radiations have been used for MS samples sterilization.

2.3. Scaffolds characterization

Fourier transformed infrared spectroscopy—FTIR, Scanning electron microscopy—SEM, Energy Dispersive Spectroscopy—EDS and X-ray Diffraction—XRD.

In order to perform FTIR analysis (Bio-Rad Win-IR Instrument, USA), samples from the scaffolds have been crushed and the obtained powder has been mixed with KBr pressed into a disk and scanned within the range of 400–4000 cm^{-1}. The cross-section morphology of scaffolds has been studied by SEM using a TESCAN-VEGA device at a current of 30 kV and local chemical analysis was performed by EDS (Oxford Instruments, UK). X'pert Pro MPD/Cubic Fast (Almelo, The Netherlands) was used for XRD analysis, performed at the following parameters: monochromatic Kα radiation (λ = 1.54056 Å), StepScan mode (0.035 s-1 scan rate), scanning angle (2θ) – between 10° and 60° and 40 mA anodic current.

Table 1
Details of the experimental program.

Scaffold	Col, (%)	Cs, (%)	Ca/P
MS1	35	65	1.6
MS2	65	35	1.6
MS3	35	65	1.7
MS4	65	35	1.7
MS5	28.79	71.21	1.65
MS6	71.21	28.79	1.65
MS7	50	50	1.579
MS8	50	50	1.721
MS9	50	50	1.65
MS10	50	50	1.65
MS11	50	50	1.65
MS12	50	50	1.65
MS13	50	50	1.65

2.4. X-ray micro-computed tomography (x-CT)

Scaffolds have been scanned using a Skyscan 1174 Compact Micro-CT system at 25 kV, 130 μA and a rotation of 0.5°, the obtained projections being refined and reconstructed with fast volumetric reconstruction software. In order to assess scaffolds porosity three regions of interest have been selected, using the sphere-fitting method from the BatMan application of the CTAn program. A transfer function of the pore size distribution was overlapped on the sample structure and colour coded, the pore size within the samples being observed as colour function.

2.5. Mechanical tests

TA-XT2 Plus (Stable Microsystems, UK) texture analyser has been used for axial compression tests and Young modulus was calculated according to Hooke's law. MS samples (0.8 mm height and 12 mm diameter) have been tested for 60 s at an initial fast deformation of 20% (1 mm/s speed) kept constant during the procedure, 1 mm/min, ambient temperature) according to the ISO 604 standard. The study has been performed in triplicate for each scaffold, the results being reported as the average ± the standard deviation.

2.6. Magnetic properties

Magnetic susceptibility balance MSB – Auto (Geneq Inc.) has been used to study MS magnetic properties, at a magnetic field intensity (H) of 4.5 kGauss. The volume susceptibility χV, or mass susceptibility χM, parameters were used to calculate the magnetization – M:M = $\chi_m \cdot H$ (emu/g) [49]. The study has been performed in triplicate for each scaffold, the results being reported as the average ± the standard deviation.

2.7. In vitro assessment of composites magnetic scaffolds

2.7.1. Retention of simulated body fluids and in vitro degradation studies

The retention of PBS was determined with volumetric method: 5 mg of each MS has been immersed in a micro-column (QIA quickVR Spin Column 50 with a 10 mm diameter) connected to a 1 mL syringe filled with PBS and incubated for 72 h at 37 °C. Finally, the maximum retention degree was calculated with equation (1):

$$RD\ (\%) = \frac{we - w0}{w0} \times 100 \quad (1)$$

where RD (%) is the maximum the retention degree; w_0 is the initial weight of the scaffold and w_e is the equilibrium weight calculated as the sum between w_0 and w_{abs} (w_{abs} = PBS density × PBS volume retained by the MS; PBS density = 1 g/mL). The study has been performed in triplicate for each scaffold, the results being reported as the average ± the standard deviation.

For *in vitro* degradation studies 10 mg of each MS have been introduced in a dialysis membrane filled with 5 mL mixture of enzymes in PBS (1200 μg/mL 1ysozyme and 0.01% collagenase), submerged in 10 mL PBS and left at 37 °C. At each time point (2 h, 48 h and 7 days) 1 mL of PBS has been extracted (and replaced with the same volume of fresh PBS) in order to measure the amount of Cs degraded (by measuring Cs reducing ends using potassium ferricyanide-$K_3Fe(CN)_6$ method) and the amount of Col degraded using ninhydrin reagent. The study has been performed in triplicate for each scaffold, the results being reported as the average ± the standard deviation.

2.7.2. In vitro cell response

All reagents/kits used for cell culture were obtained from Invitrogen, unless otherwise indicated. SaOS-2 cells (human osteogenic sarcoma) were cultivated in Dulbecco's modified Eagle's medium containing 10,000 units/mL penicillin–10,000 μg/mL streptomycin, 2 mM L-Glutamine and 10% FCS in 75 cm^3 flasks under standard cell culture conditions (5% CO_2, 95% humidity and 37 °C). SaOS-2 cell line was maintained in humidified atmosphere, 5% CO_2 in air at 37 °C, and the culture medium was exchanged every other day. When cells reached ~80% confluence, they were trypsinized with 0.25% trypsin containing ethylenediamine tetraacetic acid (1 mm, EDTA) and used for the experiments.

The cells were seeded at a density of 0.1 × 10^5 cells/cm^3 for 3 h followed by the addition of the samples on top of the cell layer and incubation for 24 h. Subsequently, the scaffolds were transferred to a new well plate, complete medium was added, and tissue culture started. For quantitative evaluation of cell viability, lactate dehydrogenase (LDH) levels in the supernatant were determined at predetermined time points (24, 96 and 168 h) of culture using a colorimetric assay (CytoTox 96® Non-Radioactive Cytotoxicity Assay, Promega) according to the manufacturer's protocol. Alexa Fluor 488 phalloidin was used to stain the actin cytoskeleton, at the predetermined time points. Briefly, 3.7% formaldehyde was used to fix the scaffolds with cells (15 min at room temperature). After the washing step with 1 × PBS and permeabilized 0.5% Triton-X (Sigma-Aldrich) in 1 × PBS, MS samples have been incubated with the fluorescent dye for 20 min at room temperature protected from light. The cell nuclei were counterstained using Hoechst 33,342 and the samples were imaged with an inverted microscope with phase contrast system and fluorescence (Leica DM IL Led). The study has been performed in triplicate for each scaffold, the results being reported as the average ± the standard deviation.

2.8. In vivo assessment

Male Wistar rats (mean body weight: 165 g, n = 40), divided into four groups, were used in order to study *in vivo* inflammatory response to MS. The animals were fed ad libitum. All animal procedures were performed in accordance with the guidelines of the ISO 10993–2 - animal welfare requirements, to ethical regulations and with the approval of the Ethics Committee of the Grigore T. Popa University of Medicine and Pharmacy, Iasi. The surgical procedures were done under thiopental anaesthesia. After removing the hair and disinfecting the rat skin with Betadine, an insertion area was made on the right flank. A surgically created pocket (1 cm diameter) was made between hypodermis and dermis, in order to insert the MS sample. All animals were subcutaneously implanted with 1 cm^2 MS sample, except the controls. Histopathological examination was performed at predetermined time points (2, 4 and 64 days) after implantation. Tissue fragments (with or without the samples) were fixed in 10% formaldehyde solution for 7 days and then included in paraffin blocks. Paraffin embedding was done using the automatic system Biooptica CD1000, followed by Masson trichrome staining. The images were obtained using a light microscope (Axioskop 2 MOT, Carl Zeiss, Jena, Germany) at 403 magnification and analysed histomorphometrically using Image Pro Plus software (Version 6.0) (Media Cybernetics Rockville, USA).

The thickness of the capsule from the periphery of the space occupied by the implant was measured in order to study the degree of MS samples encapsulation (foreign body granuloma). The encapsulation score was performed according to ISO Standard 10,993: absent capsule – score: 0; >0.5 mm – score: 1; 0.6–1.0 mm – score: 2; 1.1–2.0 mm – score: 3; >2.0 mm – score: The differences in the mean score of the batch animals must be < 1.0 mm in order to complete the demands of the test.

2.9. Experimental program

An experimental program with two variables (proportion of Cs - reported to Col, and proportion of Ca/P ratio - reported to biopolymers weight) has been used to study the composition influence on scaffold properties (Table 1). The mathematical model from equation (2) was used to correlate the parameters with properties.

$$Y = a_0 + \sum_{i-1}^{m} a_i x_i - \sum_{\substack{i-1 \\ j>1}}^{m-1} a_{ij} x_1 x_j + \sum_{i=1}^{m} a_{ij} x_i^2 - \ldots \quad (2)$$

where a_i are the regression coefficients and x_i,x_j are the input variables (Col (%), Ca/P) which influence the response variable Y (PBS retention, %; E (MPa); Magnetic susceptibility (emu/g) - Supplementary Table S1). These functions were estimated and the regression coefficients determined.

2.10. Statistical analysis

Statistical analysis was performed in GraphPad Prism v. 6.0 (GraphPad Software, Inc., La Jolla, CA). Data were analysed using two-way ANOVA with Tukey's post hoc analysis to detect significant effects of the variable. In all analyses, $p < 0.01$ was considered significant to minimize the potential for false positives owing to multiple testing.

3. Results and discussion

3.1. Scaffolds preparation

MS have been prepared by combining the biopolymers Col, Cs and Hya with different volumes of $CaCl_2$ and $NaH_2PO_4{\cdot}H_2O$ solutions (with a theoretical Ca/P ratio from 1.579 to 1.721), in the presence of SPIONs. Fig. 1 summarises the stages of the MS manufacture process.

3.2. FTIR and XRD analysis

The FTIR spectra for MS before and after sterilization (UV exposure), presented in Fig. 2A, showed absorption bands characteristic of the CP (including hydroxyapatite), biopolymers and SPIONs. The $(PO_4)^{3+}$ ions absorption peaks in the apatite phase appear as a typical doublet at 561 $cm^{-1}$and 603 cm^{-1}. The specific peaks of the $(HPO_4)^{2-}$ substituted ions occur at 875 cm^{-1} [50]. Magnetite particles are highlighted by the presence of Fe–O band at 561 cm^{-1} [51].

The characteristic absorption bands of Col occur as follow: –OH valence vibrations – 3420 cm^{-1}; -C-H of $–CH_2$ valence vibrations– 2927 cm^{-1}; Amide I– 1654 cm^{-1}; 1452 cm^{-1}; Amide III – 1244 cm^{-1} [52]. Absorption bands for Cs appear at 3420 cm^{-1} (-OH absorption), the peak at 2927 cm^{-1} is correlated to the $–CH_2$, the band at 1654 cm^{-1} is related to the amide I, the C–N stretch occur at 1313 cm^{-1} and the C–O vibration at 1028 cm^{-1}. Noteworthy to mention that UV sterilization had not modified MS composition (Supplementary data Figure S1).

The nature of the components in the inorganic layer was assessed by X-ray diffraction analysis (Fig. 2B). Phase determinations were made using Standard International Centre for Diffraction Data (ICDD) card no. 009–0432 for hydroxyapatite/calcium phosphates and 65–3107 for magnetite particles. The diffraction patterns of the MS composites can be indexed to the (002), (210), (112), (301), (310), (222) (213) and (004) planes of a cubic cell (ICDD card no.009–0432) pattern for hydroxyapatite. The main CP type within the MS composites is represented by hydroxyapatite ($Ca_{10}(PO_4)_6(OH)_2$). Moreover, the biomimetic conditions (e.g. temperature and physiological pH) used in the fabrication of MS composites lead to the formation of CP crystals.

Specific planes for magnetite (ICDD card no.65–3107) can be observed within the MS composite e.g. (220), (331), (400), (422) and (511). XRD data revealed that the MS composites contain both CP and SPIONs, supporting also the FTIR data. EDS spectrum exhibited signals related to oxygen, nitrogen, calcium, phosphorous and iron associated with the MS composition (Supplementary data Figure S2).

3.3. Magnetic and mechanical properties

The MS magnetization (M, emu/g) is presented in Fig. 3. The values obtained (ranged between 22.42 emu/g and 66.76 emu/g) are within the recommended values for application in magnetically stimulated materials for bone regeneration [34,53].

The scaffolds used for bone regeneration should fulfil several requirements, including suitable mechanical properties in order to influence specific cell functions within the given tissues [19]. Therefore, MS were subjected to compression stress and the Young modulus values (Fig. 3) varies between 70 N/m^2 and 275 N/m, the highest values being obtained for materials with higher Col concentration (specifically MS2>MS1, MS4>MS3, MS6>MS5). The decrease of Young modulus values within the MS composites could be correlated to the increasing amount of Cs in the scaffold.

Internal architecture is a key factor for a bone scaffold, as the mechanical properties can be different due to the internal structure (isotropic vs anisotropic). In the same time, scaffold morphology, pores dimension and distribution contribute to compression strength and modulus but also would create a favourable environment for cell proliferation [54,55].

3.4. Scaffolds morphology

Scaffold porosity affects mechanical properties, biological fluids absorption and biodegradability of a scaffold as the porous microstructure of a 3D scaffold could provide an appropriate environment for cell

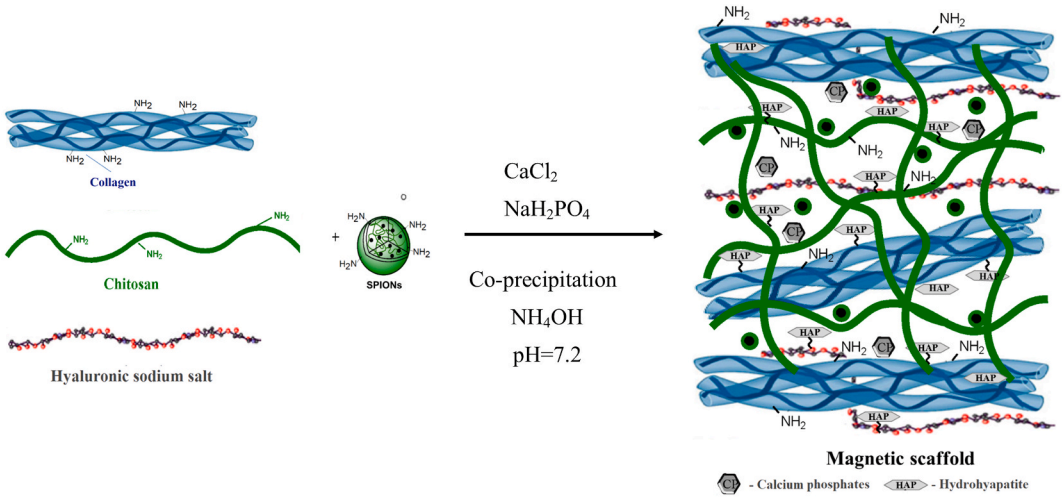

Fig. 1. Schematic steps of MS fabrication by precipitation of calcium phosphates on biopolymers and SPIONs.

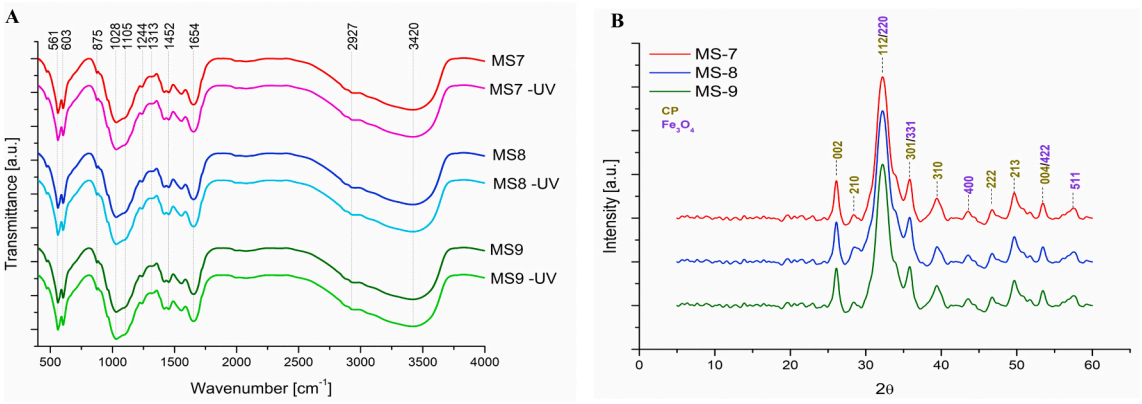

Fig. 2. A-FTIR spectra of scaffolds before and after UV exposure and B-XRD diffractograms for most representative MS (MS7, MS8 and MS9); CP-calcium phosphates, Fe_3O_4-magnetite.

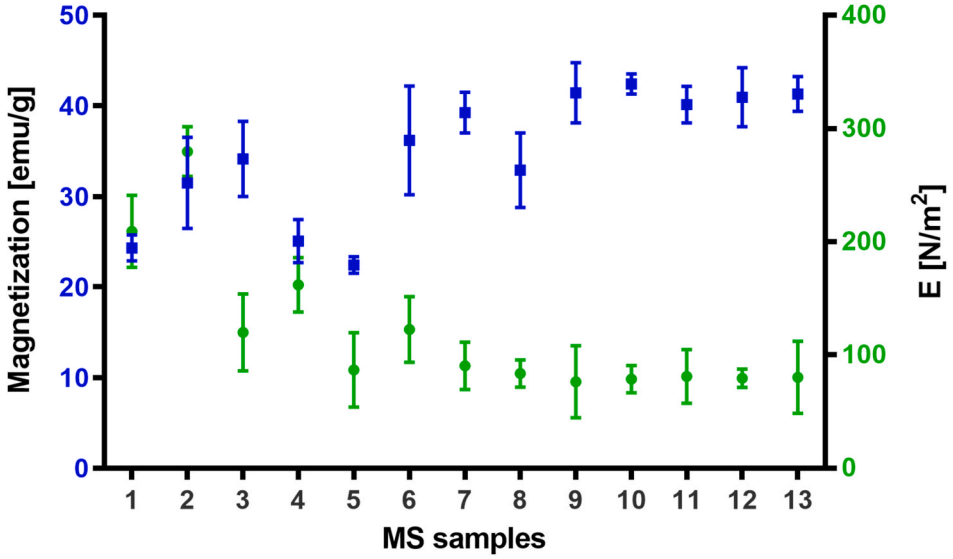

Fig. 3. Magnetization and mechanical data for MS composites; n = 3.

growth, deposition of growth factors, encapsulation of drug molecules, nutrients exchange and oxygen diffusion [56].

SEM micrographs of the MS, presented in Fig. 4 and Supplementary data Figure S1, showed a 3D architecture with highly porous interconnecting network. The internal structure of the MS composites has been evaluated by μCT and the reconstructive images are presented in Fig. 5. The μCT analysis confirmed the porous architecture of the scaffold with a pore size distribution linked to the final MS composition (Table 1).

These findings suggest that the mineral phase within the MS composites plays an essential role in developing the scaffolds architecture/morphology during freeze-drying process together with the biopolymer composition. By tailoring the composition of the organic phase (Cs and Col) whilst the inorganic phase is kept constant (Ca/P ratio) it can be observed that the pore size distribution histograms is shifted towards the highest values (MS5 vs MS6). This variation of the organic composition affected the nucleation process during the freezing procedure which generates scaffolds with an average pore size from 167.79 μm to 212.1 μm. For MS7, MS8 and MS9 the organic phase is kept constant at 50:50 (%, Cs:Col) whilst the inorganic phase (Ca/P ratio) varies between 1.579 and 1.721 (Table 1).

In these conditions, we analysed the effect of the Ca/P ratio over the final pore size of the MS. This analysis showed that a lower Ca/P ratio (1.579) will interfere with the freezing temperature of the slurry forming big ice crystal that through sublimation process will generate larger pore size within the final scaffold structure. Therefore, by increasing the Ca/P ratio the average pore size of the MS decreases. This process could be correlated with the precipitation of the inorganic phase on the biopolymer fibres implying that the pore size of the scaffold could be also tailored through changes of the Ca/P ratio.

3.5. *In vitro retention of simulated body fluids and scaffolds degradability*

Bone scaffolds need to retain their structural stability in the human body environment. Understanding the PBS uptake properties for a 3D scaffold can help correlate their properties with the prospective *in vitro* behaviour. Furthermore, the retention behaviour of the scaffolds can influence *in vitro* cell response together with distribution of nutrients, oxygen, glucose and metabolic wastes and induce cell adhesion, growth and differentiation [57]. The retention degree values obtained for MS composites are presented in Fig. 5. Noteworthy to notice, that all MS composites exhibited very high values for PBS uptake (e.g. 1000%–2500%). This can be explained through the hydrophilicity of the biopolymers exhibiting polar functional groups [58] and the porous structure of the 3D scaffolds.

Initially, the PBS molecules diffuse into the scaffolds through the pores and fill-up the inner areas. Hence, the 3D microporous structure is a critical factor for water retention within a 3D scaffold. After the first

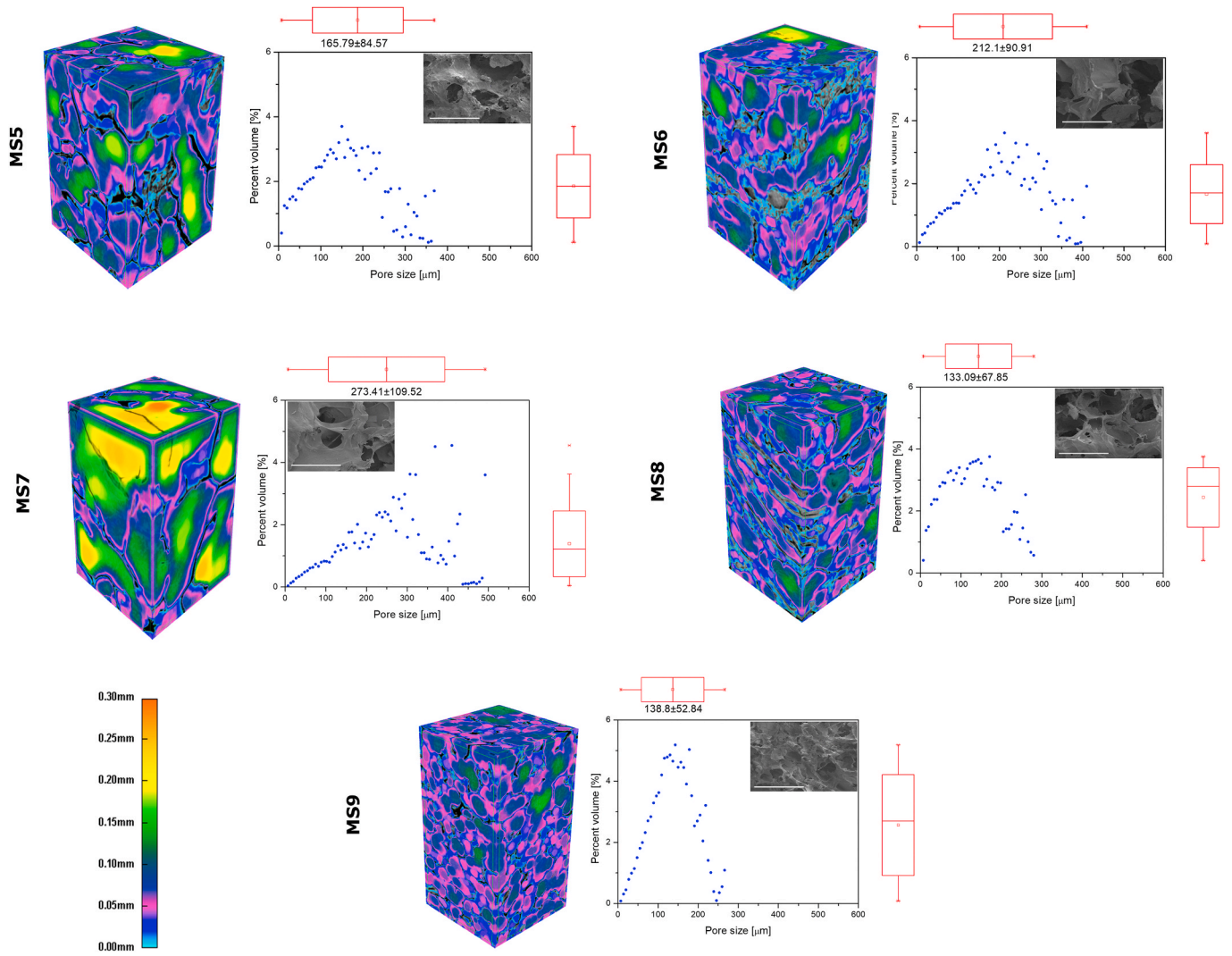

Fig. 4. X-ray micro-computed tomography, pore size distribution histograms and SEM images for most representative MS; MS5, MS6, MS7, MS8 and MS9 (false coloured pore size distribution is superimposed upon the scaffold structure); SEM scale bar-300μm; n = 3.

rapid diffusion of the PBS solution into the porous structure of the 3D scaffolds, osmotic pressure decrease. Subsequently, the scaffolds started to absorb the solution initially at a slower rate until reach the equilibrium state. On the other hand, the number of polar groups - a characteristic of all natural polymers is also an important factor which affects the material hydrophilicity [59].

The addition of the CP in scaffold composition resulted in a decrease of the swelling degree, suggesting that the MS composite materials are more stable in aqueous environment. Furthermore, an increase of swelling retention was observed in MS scaffolds with increased content of Cs and high Ca/P ratio (Fig. 5). This can be explained by the arrangement between the polymeric complex and inorganic phase, achieved through binding calcium and phosphate to the hydrophilic COOH or NH_2 groups. This result is in agreement with similar effects noticed for mixtures of collagen, pectin and hydroxyapatite [60].

Biodegradation behaviour of 3D microporous scaffolds plays an important role in the developing process of a new tissue, as the degradation rate of the scaffolds influences cell viability, cell growth, and even host response [61]. Biodegradation is a complex process occurring in different ways: by enzymatic or cellular mechanism a material disintegrates into simpler components, by elementary physical breakdown or by chemical erosion [62]. Scaffolds based on natural polymers are mainly biodegraded in the human body by particular enzymes such as, collagenase, lysozyme, or hyaluronidases and their biodegradation products are absorbed by the body [63]. On the other hand, biodegradation of calcium phosphates occurs by extracellular liquid dissolution and cell-mediated resorption, meaning that is quite difficult to be monitored *in vitro* [62].

Biodegradation of 3D composite scaffolds can be studied *in vitro* using two methods: a direct one (quantitative) which analyse the weight of the scaffolds before and after a degradation test and an indirect one (qualitative) that study the release profile of the resulted biodegradation components [64]. Considering all these aspects, the degradation behaviour of MS composites has been studied *in vitro*, in a mixture of lysozyme and collagenase [65].

The degradation kinetics of MS composites was studied for 7 days and the results are shown in Fig. 6. The degradation of the MS is detectable, even at lower time points (4 h) and the degradation rate is increasing in time at different rates. For the degraded Cs (Fig. 6A) the pattern of degradation could be explained by the presence of hexameric binding site in lysozyme that can bind to partially acetylated Cs [66,67]. The degradation pattern of the MS composites is not correlated with the amount of Cs from the scaffolds due to the ionic interactions between Cs, Col and CP which modifies the conformation of the binding site for lysozyme.

A second part of biodegradability studies involved the use of bacterial collagenase, a specific enzyme for Col, which preferentially hydrolyzes the X-Gly bonds in the following amino acid groups: glycine-

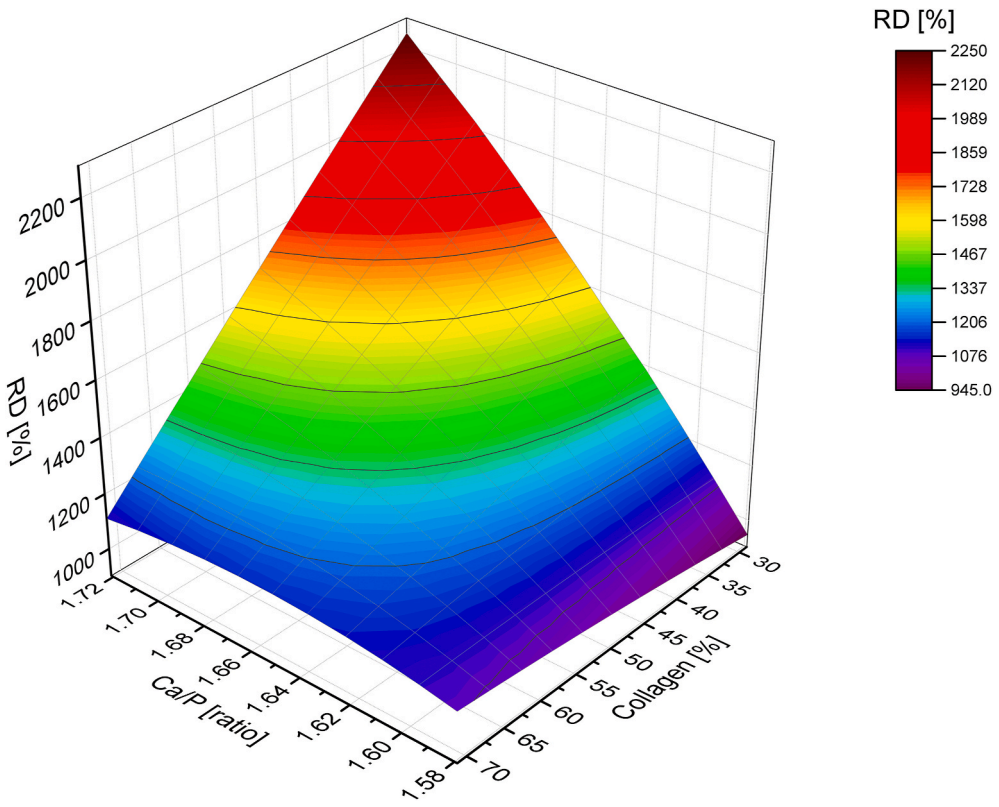

Fig. 5. 3D plot details of the PBS retention degree (RD, %) for MS composites.

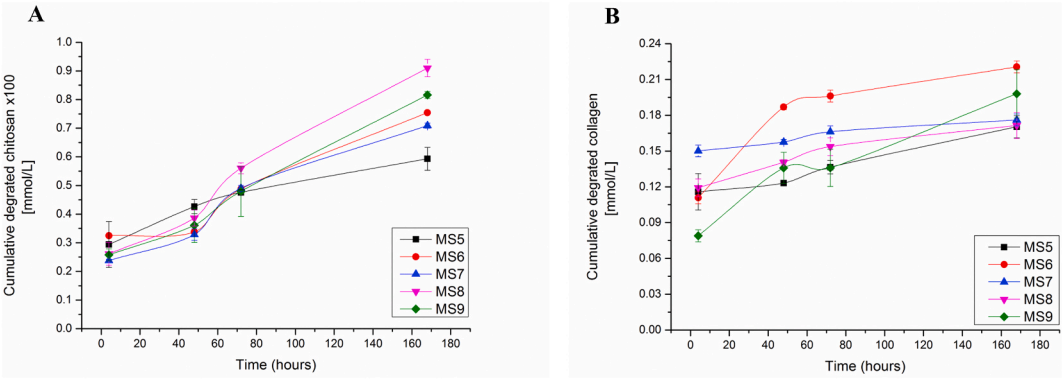

Fig. 6. *In vitro* degradation data for degraded A-Cs and B-Col from the MS composites; n = 3.

leucine (Gly-Leu), glycine-isoleucine (Gly-Ile), alanine-proline-glycine (Ala-Pro-Gly) [68,69].

The collagenase catalysed hydrolysis of the Col from MS composites in two steps: first, the enzyme attaches to the scaffold and then breaks it at specific sites corresponding to the abovementioned amino acid groups. Environmental conditions (pH, ionic strength, enzyme inhibitors) and material characteristics (composition, supramolecular structure, and porosity) dictate the degradation rate of the final MS composites. All MS were degraded in time at different rates (Fig. 6B). The MS composites with highest content of Col (e.g. MS2, MS4, MS6) exhibited an elevated degradation level (Supplementary data Figure S3).

3.6. *In vitro cell behaviour*

The cell toxicity assays demonstrate the absence of cytotoxicity of a biomaterial and allowed both qualitative and quantitative assessment of cytotoxicity. According to the ISO 10993 a biomaterial is believed to be non-cytotoxic if the cell viability is higher than 70% compared to the viability of the control sample [70,71]. A 3D scaffold biomaterial with porous structure is able to stimulate cell proliferation and to act as a template structure for neo-tissue formation. An ideal scaffold must be non-toxic, biologically active, biodegradable, with suitable mechanical properties, elicit a weak immune response and should promote its incorporation into the native tissue [72,73].

Cell viability is one of the initial assessments that can be performed in order to establish the cytotoxicity effects of a biomaterial. Quantification of cell viability by the release of LDH (Fig. 7) revealed that LDH levels at day 1 and 4 were comparable with the control group samples (TCP). This indicates that the samples have a minimum cytotoxic effect on the SaOS-2 cells. However, after 7 days in culture the LDH release from MS7 and MS8 dropped below 60% indicating a significant cytotoxic effect over the SaOS-2 cells. For MS9 samples, the LDH assay showed that the composites have a similar activity compared with the control samples. In some circumstances the values for cell viability for

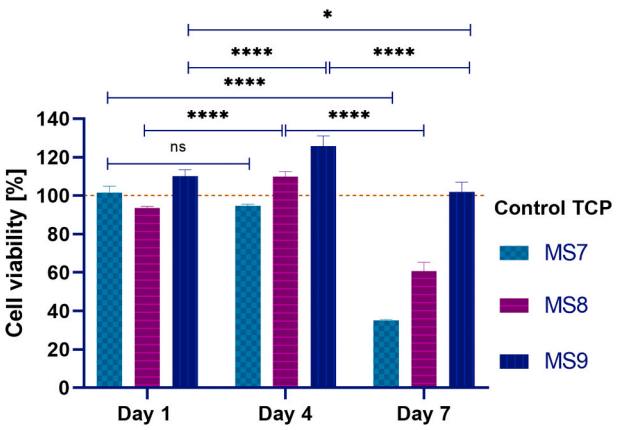

Fig. 7. Cell viability of SaOS-2 on MS composites using LDH assay; **p < 0.01, ***p < 0.001, ****p < 0.0001; n = 3.

MS8 and MS9 are above 100% indicating a better cell viability compared with the control TCP.

The results from the LDH assessment match the fluorescent staining, for actin and DAPI (Fig. 8), and bright field images (Supplementary data Figure S4) of SaOS-2 cells evaluated at predetermined time points (1, 4 and 7 days). At day 1 the morphology of the SaOS-2 cells on control samples (TCP) presented elongated shape where cytoskeleton of individual can be observed. Similar morphology with no significant changes compares with the control can be seen for the tested samples (MS7, MS8 and MS9). At day 4 and 7 the control samples reveal a confluent cell layer where cell-cell connection can be seen. A decrease in cell proliferation and changes in cell morphology for MS7 and MS8 can be observed at day 4. Several cells did not have elongated shape, instead presented more round shape and their growth is seized by possible contact inhibition with the samples. For MS9 the morphology is comparable to the control, even though some visible areas with no cells can be seen. At day 7 both MS7 and MS8 display visible areas also with no cells compared with MS9 and control where the cells have similar morphology and coverage area. The cell behaviour response is probably affected by the interplay of various parameters from the MS composition i.e. chemical composition, solubility, size of the SPIONs and CP crystals, scaffolds porosity, etc. At this stage is difficult to distinguish between their significance. However, the preliminary assessment indicates that MS9 have similar/equal cell behaviour activity compared with the TCP control.

3.6.1. *In vivo assessment*

The body recognize all the implanted biomaterials as "non-self" therefore, a typically response from the host will be encapsulation within a connective tissue. After Hench and Best [74], if the biomaterial is: (I) toxic - the surrounding tissues die; (II) nontoxic and biologically inactive (almost inert) - fibrous tissue of variable shape and thickness occurs; (III) nontoxic and biologically active (bioactive) - a close interfacial material-biological link will be produced; (IV) non-toxic and dissolves - the surrounding tissues replace it.

The intensity and duration of the inflammatory process is strongly dependent of the architecture, chemistry composition and stability of the implant [75–77]. The foreign body reaction is well described by the presence of the foreign body giant cells alongside leucocyte population [78]. The lifespan of the foreign body reaction will be determined by the chemical and topographical properties of the implanted material [79]. Neutrophils, monocytes and the resident tissue macrophages are within the first cell types to arrive at the implantation site [76]. The attachment/activation of these cells will be influenced by the cell-substrate interaction and will control the foreign body giant cells in the effort to phagocyte the implanted substrate material or formation of the fibrous capsule controlling the cell infiltration. At this point during the healing process, fibroblasts will be leading the degradation of extracellular matrix via matrix metalloproteinase, cytokines and phagocytizing collagen and foreign particles/fragments. However, the natural wound healing process will control the thickness of the fibrous capsule during the recovery period after implantation.

Fibrous encapsulation and ingrown of the fibrous connective tissue are characterized by the presence of fibroblasts bundles stained blue in Masson's Trichrome staining. For the tested MS composites, the foreign body reaction is noticeable within the first 2 days after implantation (Fig. 9). For the MS7 and MS8 the inflammatory process has been

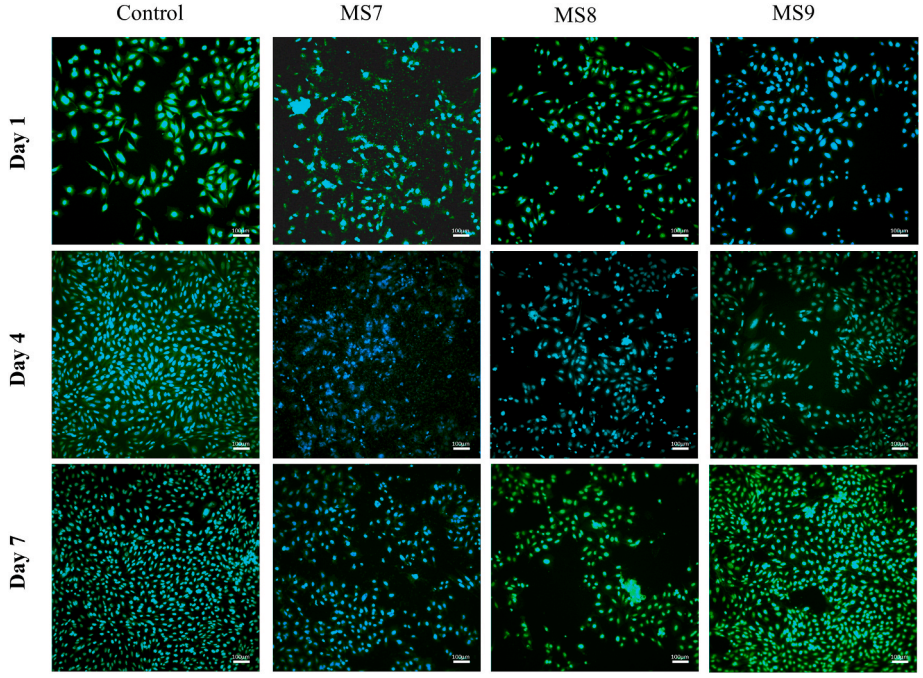

Fig. 8. Fluorescent images of SaOS-2 cells in contact with MS composites; green-AlexaFluor 488 Phallodin, Blue-nuclei stained by Hoechst 33,342; scale bar 100 μm. (For interpretation of the references to colour in this figure legend, the reader is referred to the Web version of this article.)

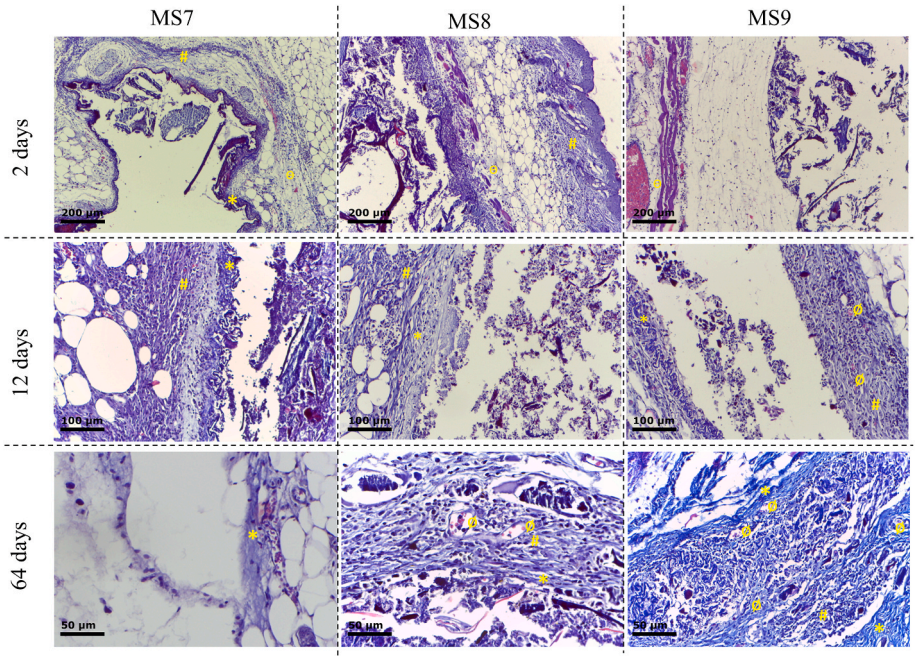

Fig. 9. Masson's trichrome staining revealing foreign body response and cellular infiltration at 2, 12- and 64-days post implantation; Θ leucocytes; Ø blood vessel, # fibroblasts and * collagen fibres.

highlighted by the presence of leucocyte (i.e. macrophages, neutrophils and rare lymphocytes), fibroblasts and collagen fibres.

However, the inflammation progression is less visible for MS9. After 12 days, both MS7 and MS8 featured fibroblast hyperplasia and deposition of extracellular matrix (collagen fibres with concentric orientation). Fibroblast proliferation and formation of new blood vessel has been visualised for MS9 at day 12. After 64 days of implantation, there is a noticeable development of integration and resorption of all MS composites with peripheral collagen production, rare leucocytes and formation of new blood vessel.

Foreign body response for the MS composites has been characterized by an acute inflammatory reaction, but its intensity decreased after the first 2 days. The thickness of the fibrous capsule was less than 0.5 mm (score 1), which positively influences material degradation and resorption over time without any significant cellular response.

4. Conclusions

A novel magnetic scaffold with 3D microstructure based on chitosan, collagen, hyaluronic acid and calcium phosphates with insertion of SPIONs was successfully fabricated through biomimetic technique. The magnetic scaffolds exhibit 3D porous structure with pores varying from 120 µm to 300 µm, as showed by µCT. Magnetization and mechanical values for all MS sets within the reported range for improving bone regeneration. The retention of PBS and *in vitro* enzymatic degradation rate is strongly correlated with the organic/inorganic phase i.e. high swelling retention was noted in MS scaffolds with increased content of Cs and high Ca/P ratio meanwhile the MS scaffolds with highest content of Col exhibited an elevated degradation level. Moreover, tailoring the composition of the organic/inorganic phase could provide control on the pore size distribution of the final MS scaffold. *In vitro* studies showed that behaviour of osteoblasts (SaOS-2) on MS9 have alike cell behaviour activity in comparison with the TCP control. *In vivo* data analysis of the tissue response to MS composites was performed in order to assess tissue ingrowth from the surrounding areas as well as evaluation of the foreign body response. There is a noticeable development of integration and resorption of all MS composites with peripheral collagen production, rare leucocytes and formation of new blood vessel up to 64 days after implantation. By tailoring the organic/inorganic phase one can achieve a 3D MS composite that could encourages tissue regeneration as the composition of the MS plays a significant role in the foreign body response. These data may have a high implication in developing magnetic scaffolds for bone regeneration and regenerative therapies.

Declaration of competing interest

The authors declare that they have no known competing financial interests or personal relationships that could have appeared to influence the work reported in this paper.

Acknowledgments

The Romanian Ministry of Research and Innovation financially supported this work; grant PN- IIPTPCCA-2013-4-2287-MAGBIOTISS.

Appendix A. Supplementary data

Supplementary data to this article can be found online at https://doi.org/10.1016/j.ceramint.2020.12.246.

References

[1] V. Campana, G. Milano, E. Pagano, M. Barba, C. Cicione, G. Salonna, W. Lattanzi, G. Logroscino, Bone substitutes in orthopaedic surgery: from basic science to clinical practice, J. Mater. Sci. Mater. Med. 25 (2014) 2445–2461.
[2] W. Wang, K.W.K. Yeung, Bone grafts and biomaterials substitutes for bone defect repair: a review, Bioact Mater 2 (2017) 224–247.
[3] G. Fernandez de Grado, L. Keller, Y. Idoux-Gillet, Q. Wagner, A.M. Musset, N. Benkirane-Jessel, F. Bornert, D. Offner, Bone substitutes: a review of their characteristics, clinical use, and perspectives for large bone defects management, J. Tissue Eng. 9 (2018), 2041731418776819.
[4] T.T. Roberts, A.J. Rosenbaum, Bone grafts, bone substitutes and orthobiologics: the bridge between basic science and clinical advancements in fracture healing, Organogenesis 8 (2012) 114–124.
[5] J.K. McEwan, H.C. Tribe, N. Jacobs, N. Hancock, A.A. Qureshi, D.G. Dunlop, R. O. Oreffo, Regenerative medicine in lower limb reconstruction, Regen. Med. 13 (2018) 477–490.
[6] J. Jeong, J.H. Kim, J.H. Shim, N.S. Hwang, C.Y. Heo, Bioactive calcium phosphate materials and applications in bone regeneration, Biomater. Res. 23 (2019) 4.
[7] S.K. Sarkar, B.T. Lee, Hard tissue regeneration using bone substitutes: an update on innovations in materials, Korean J Intern Med 30 (2015) 279–293.

[8] C.J. Kowalczewski, J.M. Saul, Biomaterials for the delivery of growth factors and other therapeutic agents in tissue engineering approaches to bone regeneration, Front. Pharmacol. 9 (2018) 513.

[9] T. Winkler, F.A. Sass, G.N. Duda, K. Schmidt-Bleek, A review of biomaterials in bone defect healing, remaining shortcomings and future opportunities for bone tissue engineering: the unsolved challenge, Bone Joint Res 7 (2018) 232–243.

[10] R. Quarto, P. Giannoni, Bone tissue engineering: past-present-future, Methods Mol. Biol. 1416 (2016) 21–33.

[11] A. Ho-Shui-Ling, J. Bolander, L.E. Rustom, A.W. Johnson, F.P. Luyten, C. Picart, Bone regeneration strategies: engineered scaffolds, bioactive molecules and stem cells current stage and future perspectives, Biomaterials 180 (2018) 143–162.

[12] J.M. Bouler, P. Pilet, O. Gauthier, E. Verron, Biphasic calcium phosphate ceramics for bone reconstruction: a review of biological response, Acta Biomater. 53 (2017) 1–12.

[13] M. Ebrahimi, M.G. Botelho, S.V. Dorozhkin, Biphasic calcium phosphates bioceramics (HA/TCP): concept, physicochemical properties and the impact of standardization of study protocols in biomaterials research, Mater Sci Eng C Mater Biol Appl 71 (2017) 1293–1312.

[14] H.L. Jang, G.B. Zheng, J. Park, H.D. Kim, H.R. Baek, H.K. Lee, K. Lee, H.N. Han, C. K. Lee, N.S. Hwang, J.H. Lee, K.T. Nam, In vitro and in vivo evaluation of whitlockite biocompatibility: comparative study with hydroxyapatite and beta-tricalcium phosphate, Adv Healthc Mater 5 (2016) 128–136.

[15] C. Feng, K. Zhang, R. He, G. Ding, M. Xia, X. Jin, C. Xie, Additive manufacturing of hydroxyapatite bioceramic scaffolds: dispersion, digital light processing, sintering, mechanical properties, and biocompatibility, Journal of Advanced Ceramics 9 (2020) 360–373.

[16] C. Tanase, A. Sartoris, M. Popa, L. Verestiuc, R. Unger, C. Kirkpatrick, In vitro evaluation of biomimetic chitosan-calcium phosphate scaffolds with potential application in bone tissue engineering, Biomed. Mater. 8 (2013).

[17] L. Kjalarsdottir, A. Dyrfjord, A. Dagbjartsson, E.H. Laxdal, G. Orlygsson, J. Gislason, J.M. Einarsson, C.H. Ng, H. Jonsson Jr., Bone remodeling effect of a chitosan and calcium phosphate-based composite, Regen Biomater 6 (2019) 241–247.

[18] S. Mooyen, N. Charoenphandhu, J. Teerapornpuntakit, J. Thongbunchoo, P. Suntornsaratoon, N. Krishnamra, I.M. Tang, W. Pon-On, Physico-chemical and in vitro cellular properties of different calcium phosphate-bioactive glass composite chitosan-collagen (CaP@ChiCol) for bone scaffolds, J. Biomed. Mater. Res. B Appl. Biomater. 105 (2017) 1758–1766.

[19] Y. Hu, J. Chen, T. Fan, Y. Zhang, Y. Zhao, X. Shi, Q. Zhang, Biomimetic mineralized hierarchical hybrid scaffolds based on in situ synthesis of nano-hydroxyapatite/chitosan/chondroitin sulfate/hyaluronic acid for bone tissue engineering, Colloids Surf. B Biointerfaces 157 (2017) 93–100.

[20] S. Stratton, N.B. Shelke, K. Hoshino, S. Rudraiah, S.G. Kumbar, Bioactive polymeric scaffolds for tissue engineering, Bioact Mater 1 (2016) 93–108.

[21] Y. Chen, N. Kawazoe, G. Chen, Preparation of dexamethasone-loaded biphasic calcium phosphate nanoparticles/collagen porous composite scaffolds for bone tissue engineering, Acta Biomater. 67 (2018) 341–353.

[22] T.M. De Witte, L.E. Fratila-Apachitei, A.A. Zadpoor, N.A. Peppas, Bone tissue engineering via growth factor delivery: from scaffolds to complex matrices, Regen Biomater 5 (2018) 197–211.

[23] N.G. Sahoo, Y.Z. Pan, L. Li, C.B. He, Nanocomposites for bone tissue regeneration, Nanomedicine 8 (2013) 639–653.

[24] C. Gardin, L. Ferroni, L. Favero, E. Stellini, D. Stomaci, S. Sivolella, E. Bressan, B. Zavan, Nanostructured biomaterials for tissue engineered bone tissue reconstruction, Int. J. Mol. Sci. 13 (2012) 737–757.

[25] G. S, G. T, V. K, A.A. Faleh, A. Sukumaran, N.S. P, Development of 3D scaffolds using nanochitosan/silk-fibroin/hyaluronic acid biomaterials for tissue engineering applications, Int. J. Biol. Macromol. 120 (2018) 876–885.

[26] S. Kuttappan, D. Mathew, M.B. Nair, Biomimetic composite scaffolds containing bioceramics and collagen/gelatin for bone tissue engineering - a mini review, Int. J. Biol. Macromol. 93 (2016) 1390–1401.

[27] S. Fu, M. Zhu, Y. Zhu, Organosilicon polymer-derived ceramics: an overview, Journal of Advanced Ceramics 8 (2019) 457–478.

[28] C.M. Brougham, T.J. Levingstone, N. Shen, G.M. Cooney, S. Jockenhoevel, T. C. Flanagan, F.J. O'Brien, Freeze-drying as a novel biofabrication method for achieving a controlled microarchitecture within large, complex natural biomaterial scaffolds, Adv Healthc Mater 6 (2017) 1700598.

[29] G.S. Offeddu, L. Mohee, R.E. Cameron, Scale and structure dependent solute diffusivity within microporous tissue engineering scaffolds, J. Mater. Sci. Mater. Med. 31 (2020) 46.

[30] G.S. Offeddu, C.E. Tanase, S. Toumpaniari, M.L. Oyen, R.E. Cameron, Stiffening by Osmotic Swelling Constraint in Cartilage-like Cell Culture Scaffolds, Macromolecular Bioscience, 2018.

[31] C. Sobacchi, M. Erreni, D. Strina, E. Palagano, A. Villa, C. Menale, 3D bone biomimetic scaffolds for basic and translational studies with mesenchymal stem cells, Int. J. Mol. Sci. 19 (2018).

[32] A.R. Amini, C.T. Laurencin, S.P. Nukavarapu, Bone tissue engineering: recent advances and challenges, Crit. Rev. Biomed. Eng. 40 (2012) 363–408.

[33] K. Dzobo, N.E. Thomford, D.A. Senthebane, H. Shipanga, A. Rowe, C. Dandara, M. Pillay, K. Motaung, Advances in regenerative medicine and tissue engineering: innovation and transformation of medicine, Stem Cell. Int. 2018 (2018) 1–24, https://doi.org/10.1155/2018/2495848, 2495848.

[34] Y. Xia, J. Sun, L. Zhao, F. Zhang, X.J. Liang, Y. Guo, M.D. Weir, M.A. Reynolds, N. Gu, H.H.K. Xu, Magnetic field and nano-scaffolds with stem cells to enhance bone regeneration, Biomaterials 183 (2018) 151–170.

[35] S. Hu, Y. Zhou, Y. Zhao, Y. Xu, F. Zhang, N. Gu, J. Ma, M.A. Reynolds, Y. Xia, H.H. K. Xu, Enhanced bone regeneration and visual monitoring via superparamagnetic iron oxide nanoparticle scaffold in rats, J Tissue Eng Regen Med 12 (2018) e2085–e2098.

[36] H.M. Yun, S.J. Ahn, K.R. Park, M.J. Kim, J.J. Kim, G.Z. Jin, H.W. Kim, E.C. Kim, Magnetic nanocomposite scaffolds combined with static magnetic field in the stimulation of osteoblastic differentiation and bone formation, Biomaterials 85 (2016) 88–98.

[37] M.A. Fernandez-Yague, S.A. Abbah, L. McNamara, D.I. Zeugolis, A. Pandit, M. J. Biggs, Biomimetic approaches in bone tissue engineering: integrating biological and physicomechanical strategies, Adv. Drug Deliv. Rev. 84 (2015) 1–29.

[38] Y. Li, D. Ye, M. Li, M. Ma, N. Gu, Adaptive materials based on iron oxide nanoparticles for bone regeneration, ChemPhysChem 19 (2018) 1965–1979.

[39] J.W. Lu, F. Yang, Q.F. Ke, X.T. Xie, Y.P. Guo, Magnetic nanoparticles modified-porous scaffolds for bone regeneration and photothermal therapy against tumors, Nanomedicine 14 (2018) 811–822.

[40] F. Xiong, H. Wang, Y. Feng, Y. Li, X. Hua, X. Pang, S. Zhang, L. Song, Y. Zhang, N. Gu, Cardioprotective activity of iron oxide nanoparticles, Sci. Rep. 5 (2015) 8579.

[41] C. Shuai, W. Yang, C. He, S. Peng, C. Gao, Y. Yang, F. Qi, P. Feng, A magnetic micro-environment in scaffolds for stimulating bone regeneration, Mater. Des. 185 (2020), 108275.

[42] D. Fan, Q. Wang, T. Zhu, H. Wang, B. Liu, Y. Wang, Z. Liu, X. Liu, D. Fan, X. Wang, Recent advances of magnetic nanomaterials in bone tissue repair, Frontiers in Chemistry 8 (2020).

[43] D.M. Huang, J.K. Hsiao, Y.C. Chen, L.Y. Chien, M. Yao, Y.K. Chen, B.S. Ko, S. C. Hsu, L.A. Tai, H.Y. Cheng, S.W. Wang, C.S. Yang, Y.C. Chen, The promotion of human mesenchymal stem cell proliferation by superparamagnetic iron oxide nanoparticles, Biomaterials 30 (2009) 3645–3651.

[44] Q. Wang, B. Chen, M. Cao, J. Sun, H. Wu, P. Zhao, J. Xing, Y. Yang, X. Zhang, M. Ji, N. Gu, Response of MAPK pathway to iron oxide nanoparticles in vitro treatment promotes osteogenic differentiation of hBMSCs, Biomaterials 86 (2016) 11–20.

[45] S. Lugert, H. Unterweger, M. Muhlberger, C. Janko, S. Draack, F. Ludwig, D. Eberbeck, C. Alexiou, R.P. Friedrich, Cellular effects of paclitaxel-loaded iron oxide nanoparticles on breast cancer using different 2D and 3D cell culture models, Int. J. Nanomed. 14 (2019) 161–180.

[46] Z.Q. Zhang, S.C. Song, Multiple hyperthermia-mediated release of TRAIL/SPION nanocomplex from thermosensitive polymeric hydrogels for combination cancer therapy, Biomaterials 132 (2017) 16–27.

[47] V. Balan, I.A. Petrache, M.I. Popa, M. Butnaru, E. Barbu, J. Tsibouklis, L. Verestiuc, Biotinylated chitosan-based SPIONs with potential in blood-contacting applications, J. Nanoparticle Res. 14 (2012) 730.

[48] F.D. Cojocaru, V. Balan, M.I. Popa, A. Lobiuc, A. Antoniac, I.V. Antoniac, L. Verestiuc, Biopolymers – calcium phosphates composites with inclusions of magnetic nanoparticles for bone tissue engineering, Int. J. Biol. Macromol. 125 (2019) 612–620.

[49] R.S. Davis, Determining the magnetic properties of 1 kg mass standards, Journal of research of the National Institute of Standards and Technology 100 (1995) 209–226.

[50] M.A. Nazeer, E. Yilgor, I. Yilgor, Intercalated chitosan/hydroxyapatite nanocomposites: promising materials for bone tissue engineering applications, Carbohydr. Polym. 175 (2017) 38–46.

[51] F. Heidari, M.E. Bahrololoom, D. Vashaee, L. Tayebi, In situ preparation of iron oxide nanoparticles in natural hydroxyapatite/chitosan matrix for bone tissue engineering application, Ceram. Int. 41 (2015) 3094–3100.

[52] L. Radev, N.Y. Mostafa, I. Michailova, I.M.M. Salvado, M.H.V. Fernandes, *In vitro* bioactivity of collagen/calcium phosphate silicate composites, cross-linked with chondroitin sulfate, Int. J. Mater. Chem. 2 (2012) 1–9.

[53] A. Bigham, A.H. Aghajanian, S. Behzadzadeh, Z. Sokhani, S. Shojaei, Y. Kaviani, S. A. Hassanzadeh-Tabrizi, Nanostructured magnetic Mg2SiO4-CoFe2O4 composite scaffold with multiple capabilities for bone tissue regeneration, Mater. Sci. Eng. C 99 (2019) 83–95.

[54] R.A. Perez, G. Mestres, Role of pore size and morphology in musculo-skeletal tissue regeneration, Mater Sci Eng C Mater Biol Appl 61 (2016) 922–939.

[55] S. Wu, X. Liu, K.W.K. Yeung, C. Liu, X. Yang, Biomimetic porous scaffolds for bone tissue engineering, Mater. Sci. Eng. R Rep. 80 (2014) 1–36.

[56] A. Hajinasab, S. Saber-Samandari, S. Ahmadi, K. Alamara, Preparation and characterization of a biocompatible magnetic scaffold for biomedical engineering, Mater. Chem. Phys. 204 (2018) 378–387.

[57] X. He, X. Fan, W. Feng, Y. Chen, T. Guo, F. Wang, J. Liu, K. Tang, Incorporation of microfibrillated cellulose into collagen-hydroxyapatite scaffold for bone tissue engineering, Int. J. Biol. Macromol. 115 (2018) 385–392.

[58] I.M. Hung, W.J. Shih, M.H. Hon, M.C. Wang, The properties of sintered calcium phosphate with [Ca]/[P] = 1.50, Int. J. Mol. Sci. 13 (2012) 13569–13586.

[59] B. Kaczmarek, A. Sionkowska, A.M. Osyczka, Physicochemical properties of scaffolds based on mixtures of chitosan, collagen and glycosaminoglycans with nano-hydroxyapatite addition, Int. J. Biol. Macromol. 118 (2018) 1880–1883.

[60] F. Wenpo, L. Gaofeng, F. Shuying, Q. Yuanming, T. Keyong, Preparation and characterization of collagen-hydroxyapatite/pectin composite, Int. J. Biol. Macromol. 74 (2015) 218–223.

[61] A. Albert, T. Lochner, T.J. Schmidt, L. Gubler, Stability and degradation mechanisms of radiation-grafted polymer electrolyte membranes for water electrolysis, ACS Appl. Mater. Interfaces 8 (2016) 15297–15306.

[62] Z. Sheikh, M.N. Abdallah, A.A. Hanafi, S. Misbahuddin, H. Rashid, M. Glogauer, Mechanisms of in vivo degradation and resorption of calcium phosphate based biomaterials, Materials 8 (2015) 7913–7925.

[63] A. Sionkowska, J. Kozlowska, Properties and modification of porous 3-D collagen/hydroxyapatite composites, Int. J. Biol. Macromol. 52 (2013) 250–259.
[64] J. Shi, M.M. Xing, W. Zhong, Development of hydrogels and biomimetic regulators as tissue engineering scaffolds, Membranes 2 (2012) 70–90.
[65] J. Shi, M.M.Q. Xing, W. Zhong, Development of hydrogels and biomimetic regulators as tissue engineering scaffolds, Membranes 2 (2012) 70–90.
[66] A.R. Costa-Pinto, A.M. Martins, M.J. Castelhano-Carlos, V.M. Correlo, P.C. Sol, A. Longatto-Filho, M. Battacharya, R.L. Reis, N.M. Neves, In vitro degradation and in vivo biocompatibility of chitosan–poly(butylene succinate) fiber mesh scaffolds, J. Bioact. Compat Polym. 29 (2014) 137–151.
[67] S.H. Pangburn, P.V. Trescony, J. Heller, Lysozyme degradation of partially deacetylated chitin, its films and hydrogels, Biomaterials 3 (1982) 105–108.
[68] L. Chung, D. Dinakarpandian, N. Yoshida, J.L. Lauer-Fields, G.B. Fields, R. Visse, H. Nagase, Collagenase unwinds triple-helical collagen prior to peptide bond hydrolysis, EMBO J. 23 (2004) 3020–3030.
[69] N. Inoue, Y. Omata, K. Yonemasu, F.G. Claveria, I. Igarashi, A. Saito, N. Suzuki, Collagen cross-reactive antigen of Sarcocystis cruzi, Vet. Parasitol. 63 (1996) 17–23.
[70] J. Carraway, C. Ghosh, The challenge to global acceptance of Part 3 of ISO 10993, Med. Device Technol. 17 (2006) 16–18.
[71] P. Sánchez, J.L. Pedraz, G. Orive, Biologically active and biomimetic dual gelatin scaffolds for tissue engineering, Int. J. Biol. Macromol. 98 (2017) 486–494.
[72] F.R. Tentor, J.H. de Oliveira, D.B. Scariot, D. Lazarin-Bidóia, E.G. Bonafé, C. V. Nakamura, S.A.S. Venter, J.P. Monteiro, E.C. Muniz, A.F. Martins, Scaffolds based on chitosan/pectin thermosensitive hydrogels containing gold nanoparticles, Int. J. Biol. Macromol. 102 (2017) 1186–1194.
[73] X. Zhang, W. Jiang, Y. Liu, P. Zhang, L. Wang, W. Li, G. Wu, Y. Ge, Y. Zhou, Human adipose-derived stem cells and simvastatin-functionalized biomimetic calcium phosphate to construct a novel tissue-engineered bone, Biochem. Biophys. Res. Commun. 495 (2018) 1264–1270.
[74] L.L. Hench, S.M. Best, Chapter I.2.4 - ceramics, glasses, and glass-ceramics: basic principles, in: B.D. Ratner, A.S. Hoffman, F.J. Schoen, J.E. Lemons (Eds.), Biomaterials Science, third ed., Academic Press, 2013, pp. 128–151.
[75] J.M. Anderson, A. Rodriguez, D.T. Chang, Foreign body reaction to biomaterials, Semin. Immunol. 20 (2008) 86–100.
[76] R. Klopfleisch, F. Jung, The pathology of the foreign body reaction against biomaterials, J. Biomed. Mater. Res. 105 (2017) 927–940.
[77] M.J. van Luyn, J.A. Plantinga, L.A. Brouwer, I.M. Khouw, L.F. de Leij, P.B. van Wachem, Repetitive subcutaneous implantation of different types of (biodegradable) biomaterials alters the foreign body reaction, Biomaterials 22 (2001) 1385–1391.
[78] R. Trindade, T. Albrektsson, P. Tengvall, A. Wennerberg, Foreign body reaction to biomaterials: on mechanisms for buildup and breakdown of osseointegration, Clin. Implant Dent. Relat. Res. 18 (2016) 192–203.
[79] A. Vishwakarma, N.S. Bhise, M.B. Evangelista, J. Rouwkema, M.R. Dokmeci, A. M. Ghaemmaghami, N.E. Vrana, A. Khademhosseini, Engineering immunomodulatory biomaterials to tune the inflammatory response, Trends Biotechnol. 34 (2016) 470–482.